ACS Chemical Neuroscience
Cite This: ACS Chem. Neurosci. 2018, 9, 1492−1502
Research Article
pubs.acs.org/chemneuro

Exploring the Binding Mechanism of Metabotropic Glutamate Receptor 5 Negative Allosteric Modulators in Clinical Trials by Molecular Dynamics Simulations

Tingting Fu,[†,‡] Guoxun Zheng,[†,‡] Gao Tu,[†,‡] Fengyuan Yang,[†,‡] Yuzong Chen,[§] Xiaojun Yao,[∥] Xiaofeng Li,[†,‡] Weiwei Xue,*[,†] and Feng Zhu*[,†,‡]

[†]Innovative Drug Research and Bioinformatics Group, School of Pharmaceutical Sciences, and Collaborative Innovation Center for Brain Science, Chongqing University, Chongqing 401331, China

[‡]Innovative Drug Research and Bioinformatics Group, College of Pharmaceutical Sciences, Zhejiang University, Hangzhou 310058, China

[§]Bioinformatics and Drug Design Group, Department of Pharmacy, National University of Singapore, Singapore 117543, Singapore

[∥]State Key Laboratory of Applied Organic Chemistry and Department of Chemistry, Lanzhou University, Lanzhou 730000, China

Supporting Information

ABSTRACT: Metabotropic glutamate receptor 5 ($mGlu_5$) plays a key role in synaptic information storage and memory, which is a well-known target for a variety of psychiatric and neurodegenerative disorders. In recent years, the increasing efforts have been focused on the design of allosteric modulators, and the negative allosteric modulators (NAMs) are the front-runners. Recently, the architecture of the transmembrane (TM) domain of $mGlu_5$ receptor has been determined by crystallographic experiment. However, it has been not well understood how the pharmacophores of NAMs accommodated into the allosteric binding site. In this study, molecular dynamics (MD) simulations were performed on $mGlu_5$ receptor bound with NAMs in preclinical or clinical development to shed light on this issue. In order to identify the key residues, the binding free energies as well as per-residue contributions for NAMs binding to $mGlu_5$ receptor were calculated. Subsequently, the *in silico* site-directed mutagenesis of the key residues was performed to verify the accuracy of simulation models. As a result, the shared common features of the studied 5 clinically important NAMs (mavoglurant, dipraglurant, basimglurant, STX107, and fenobam) interacting with 11 residues in allosteric site were obtained. This comprehensive study presented a better understanding of $mGlu_5$ receptor NAMs binding mechanism, which would be further used as a useful framework to assess and discover novel lead scaffolds for NAMs.

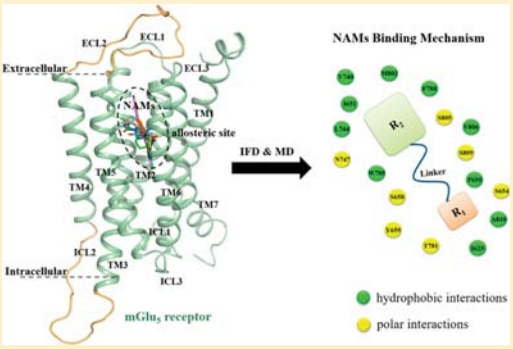

KEYWORDS: *Metabotropic glutamate receptor 5, psychiatric and neurodegenerative disorders, negative allosteric modulators, molecular dynamics, drug design*

INTRODUCTION

Metabotropic glutamate receptor 5 ($mGlu_5$), a subtype of the metabotropic glutamate family, belongs to class C G-protein-coupled receptors (GPCRs).[1,2] It is widely distributed in the central nervous system (CNS)[3,4] and plays a key role in synaptic information storage and memory.[5] It is well-known that the $mGlu_5$ receptor is an important pharmaceutical target for developing the effective therapeutics for various disorders,[6−9] such as fragile X syndrome (FXS),[10−12] Parkinson's disease levodopa-induced dyskinesias (PD-LID),[13,14] obsessive-compulsive disorder (OCD),[15] and major depressive disorder (MDD).[16,17] The structure of $mGlu_5$ consists of a large extracellular domain with an orthosteric site and a seven transmembrane (7TM) α-helice domain with an allosteric site.[18] For the type of receptor, the subtype selectivity, non-drug-like properties, limited CNS exposure, and lack of efficacy[19−21] have rendered great challenges for the classical strategies[22] of target modulation via orthosteric sites. To address these major limitations, increasing efforts have been focused on discovering allosteric modulators (PAMs, NAMs, and SAMs), which were demonstrated to show good pharmacokinetic property and subtype selectivity.[23−25]

Among all these $mGlu_5$ receptor allosteric modulators, negative allosteric modulators (NAMs) are the front-runners,[26] like dipraglurant approved by the United States Food and Drug Administration (FDA) as an orphan drug for PD-LID in 2016.[27] In addition, several NAM drug candidates were stepping into the pipeline of clinical development, such as

Received: February 8, 2018
Accepted: March 9, 2018
Published: March 9, 2018

DOI: 10.1021/acschemneuro.8b00059
ACS Chem. Neurosci. 2018, 9, 1492−1502

mavoglurant, basimglurant, and fenobam (Table 1).[28−32] In spite of the promising results obtained from previous studies for NAM development, they were still faced with the "shallow" or "flat" structure−activity relationship (SAR), making it difficult to optimize drug parameters.[33−35] Hence, there is an urgent need to unambiguously understand the ligand−receptor interactions and thus to improve the scaffolds diversity of NAMs.[36−39] To our best knowledge, the docking and molecular dynamics (MD) analysis based on homology modeling as a useful tool have been reported to be applied to study the interactions between $mGlu_5$ receptor and some NAMs,[40−42] but the more comprehensive understanding of binding mechanism of NAMs binding to $mGlu_5$ receptor is still lacking. Recently, the high-resolution crystal structures of $mGlu_5$ transmembrane (TM) domain with NAMs crystallized in the allosteric site have been determined, which provides a new higher starting point to further understand the binding mechanism of NAMs to the $mGlu_5$ receptor.[1,37,43]

Table 1. Information of Five Clinically Important NAMs Studied in This Work[a]

NAM	disease	clinical phase	organization
mavoglurant	OCD	phase II	Novartis
	FXS	discontinued	Novartis
	PD-LID	discontinued	Novartis
dipraglurant	PD-LID	as an orphan drug granted by FDA	Addex
basimglurant	MDD	phase II	Roche
	FXS	discontinued	Roche
STX107	FXS	phase II	Seaside Therapeutics
fenobam	FXS	phase II	Autism Therapeutics

[a]Information collected from the www.clinicaltrials.gov and refs 15, 19, 27, and 96.

In this work, the binding mechanism of eight $mGlu_5$ receptor NAMs (Figure 1) including five acetylene ligands (mavoglurant, dipraglurant, basimglurant, STX107, and MPEP), and three nonacetylene ligands (fenobam, 51D, and 51E) was explored by integrating multiple computational methods. First, the initial poses of NAMs in $mGlu_5$ receptor were obtained by Induced Fit Docking (IFD) approach and were further assessed by molecular dynamics (MD) simulation and end-point binding free energy (BFE) calculation. Then, the simulation model was validated by *in silico* site-directed mutagenesis analysis. Finally, a binding mode shared by the clinically important NAMs (mavoglurant, dipraglurant, basimglurant, STX107, and fenobam) was identified by clustering per-residue binding free energy contribution. The structural and energetic profile identified in this study provided important insights into the binding mechanism of approved or clinical NAMs, which could be further utilized as a useful framework to assess and discover novel lead scaffolds.

RESULTS AND DISCUSSION

Initial Binding Poses of NAMs Predicted by Induced Fit Docking. Based on the modified crystal structure of mavoglurant-$mGlu_5$, the IFD approach was carried out to predict initial poses of five NAMs (dipraglurant, basimglurant, STX107, fenobam, and MPEP) binding to the $mGlu_5$ receptor. A list of 20 top-ranked poses were obtained for each NAM from IFD, and the poses of studied NAMs with the most similar orientation of original mavoglurant were selected (Supporting Information (SI), Figure S1). As shown, all the NAMs were located in allosteric binding site surrounded by TM2, TM3, TM5, TM6, and TM7. Meanwhile, the obtained redocking pose of mavoglurant kept consistence with the crystallized conformation (SI, Figure S2). The superimpositions of ligands (heavy atoms) and binding site residues (backbone atoms) between the docking and crystallized structures were evaluated via root mean square deviation (RMSD) with the values of 0.17 and 0.33 Å, respectively. As a result, the redocking study validated the reliability of the IFD approach and guaranteed the correct initial poses of the five studied NAMs generated in this work.

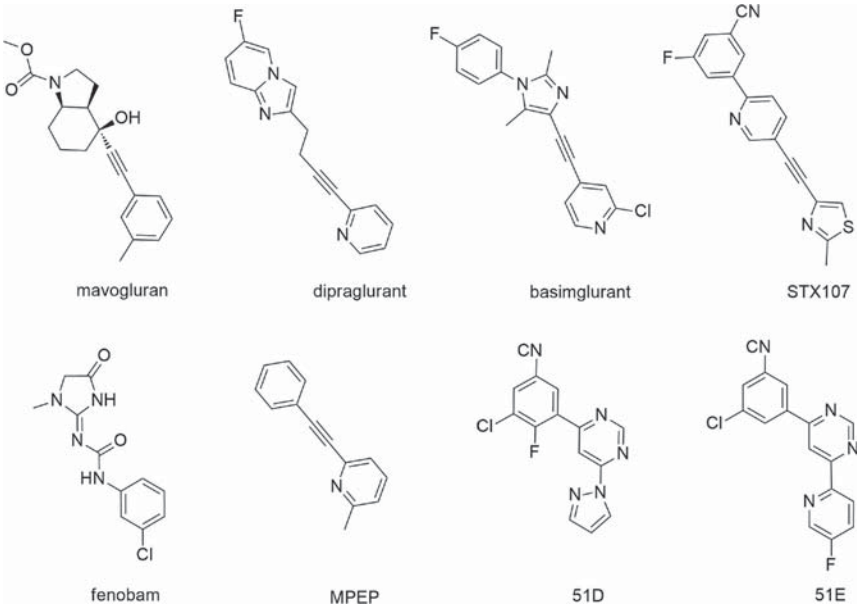

Figure 1. Chemical structures of the eight studied NAMs in this work.

DOI: 10.1021/acschemneuro.8b00059
ACS Chem. Neurosci. 2018, 9, 1492−1502

Assessment of the NAMs Binding to the $mGlu_5$ Receptor. *Ability of MD Simulation to Judge and Optimize the Binding Poses.* MD simulation of 100 ns was performed for each system. The stabilities of NAM binding to $mGlu_5$ receptor under simulation were evaluated by comparing RMSD values (SI, Figure S3) of protein backbone atoms, ligand heavy atoms, and backbone atoms of binding site residues (around 5.0 Å of the ligand) with the corresponding poses from crystal structures or docking. As shown, the RMSDs of binding sites and ligands underwent a small displacement (RMSD < 2.0 Å). The average RMSD values of the intra- and extracellular loops in eight studied complexes were 2.86−3.22 Å. Therefore, the relatively large protein RMSDs (2.0 Å < RMSD < 4.0 Å) shown in SI, Figure S3 were mainly due to the intra- and extracellular loops of the receptors. Moreover, the calculated root mean square fluctuation (RMSF) versus the protein residue numbers of $mGlu_5$ demonstrated that the IL2 and EL2 loops in the receptor underwent relatively large fluctuations during the simulation (SI, Figure S4).

As shown in SI, Figure S3, it was observed that the conformations of five NAMs (dipraglurant, basimglurant, STX107, fenobam, and MPEP) from docking were less stable than those of three NAMs (mavoglurant, 51D, and 51E) from crystal structures at the first 20 ns simulation. The close views of the alignments of representative snapshots of NAMs-$mGlu_5$ receptor complexes from the equilibrated trajectories to their corresponding initial conformations are displayed in SI, Figure S5. It was shown that the poses of mavoglurant, 51D, and 51E from MD trajectory overlapped very well with the crystal poses, and a slight shift was observed for the docking poses of dipraglurant, basimglurant, STX107, fenobam, and MPEP against the MD poses. This phenomenon observed herein indicated that the MD simulations sufficed to judge and optimize the binding poses of studied NAMs binding to $mGlu_5$ receptor, especially in the final 50 ns. Therefore, the last 50 ns equilibrated trajectories were adopted to estimate the thermodynamic profiles of NAMs binding to $mGlu_5$ receptor and further analyze the interactions between them.

Profiles of Binding Free Energies. Binding free energies (ΔG_{calc}) of NAMs to $mGlu_5$ receptor were calculated by the MM/GBSA method[44,45] and then compared with experimental binding affinities (ΔG_{exp}). ΔG_{exp} was estimated based on the reported K_i values[29,37,41] via $\Delta G_{exp} = RT\ln(K_i)$. As shown in Table 2, the values of ΔG_{calc} were −39.66, −38.84, −32.71, −37.80, −43.30, and −44.90 kcal/mol for mavoglurant, basimglurant, fenobam, MPEP, 51D and 51E complexes, respectively, which were all higher than those of the experimental ones. This was because of the approximations inherent to the MM/GBSA method, which was more applicable for ranking of ligand binding affinities rather than quantitatively predicting absolute binding free energies.[46,47] The calculated relative binding free energies ($\Delta\Delta G$) with fenobam as a reference indicated a good correlation (R^2 = 0.90) between the calculated and experimental values in Figure 2. The detailed contributions of each energy components in eq 1 are illustrated in SI, Table S1. As shown, the binding of NAMs to $mGlu_5$ receptor was mainly contributed by van der Waals (ΔE_{vdW}) and electrostatic interactions (ΔE_{ele}), but impeded by polar solvent energy (ΔG_{pol}). Taking basimglurant complex as an example, the ΔE_{vdW} (−52.49 kcal/mol) and ΔE_{ele} (−18.24 kcal/mol) were favorable to its binding, but the ΔG_{pol} (37.44 kcal/mol) was harmful to binding.

Table 2. Calculated and Experimental Data of Eight NAMs Binding to $mGlu_5$ Receptor (ΔG is in kcal/mol and K_i Value is in nM)

NAMs	K_i [a]	ΔG_{exp} [b]	$\Delta\Delta G_{exp}$ [c]	ΔG_{calc} [d]	$\Delta\Delta G_{calc}$ [c]
mavoglurant	10	−11.34	−1.72	−39.66	−6.95
dipraglurant				−41.76	−9.05
basimglurant	36	−10.55	−0.93	−38.84	−6.13
STX107				−46.12	−13.41
fenobam	162.2	−9.62	0.00	−32.71	0.00
MPEP	10.4	−11.31	−1.69	−37.80	−5.09
51D	0.501	−13.18	−3.56	−43.30	−10.59
51E	0.501	−13.18	−3.56	−44.90	−12.19

[a] K_i values obtained from previous studies.[29,37,41] [b] Estimated binding affinities based on K_i values by the equation $\Delta G_{exp} = RT\ln(K_i)$, where R = 8.314 J/(mol·K) and T = 310.0 K. [c] $\Delta\Delta G$ is defined as the change of binding free energy using fenobam as a reference. [d] Calculated MM/GBSA binding free energies in this work.

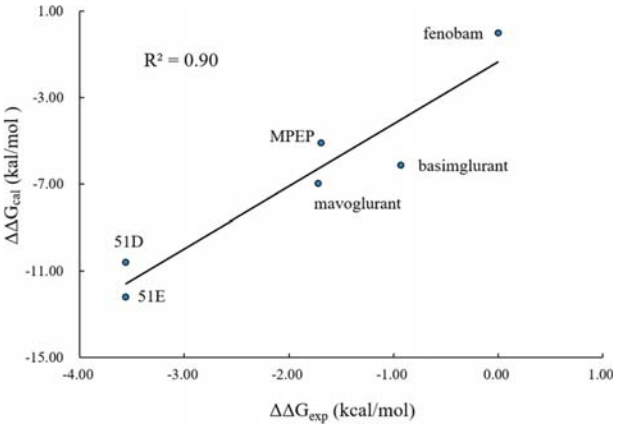

Figure 2. Correlation between the calculated binding energy differences ($\Delta\Delta G_{calc}$) and that of experiment ($\Delta\Delta G_{exp}$) for NAMs bound complexes.

In Silico Site-Directed Mutagenesis Analysis. So far, only experimental mutagenesis data was reported for MPEP.[48,49] To verify the MD simulated models in this work, *in silico* site-directed mutagenesis analysis was conducted on the MPEP bound complex. As the first probe ligand of NAMs, several mutational experiments[48,49] indicated that the residues ($P654^{3.36}$, $S657^{3.39}$, $Y658^{3.40}$, $L743^{5.47}$, $T780^{6.44}$, and $Y791^{6.55}$) were sensitive to MPEP binding to rat $mGlu_5$ receptor. Therefore, the corresponding residues ($P655^{3.40}$, $S658^{3.43}$, $Y659^{3.44}$, $L744^{5.44}$, $T781^{6.46}$, and $Y792^{6.57}$) in human $mGlu_5$ receptor were selected for *in silico* mutagenesis analysis and then the calculated results were compared with the mutational experiments. The RMSD values of seven mutants (P655S, S658C, P655S-S658C, Y659F, L744V, T781A, and Y792A) under additional short MD simulation (20 ns) are shown in SI, Figure S6, and the binding free energy changes and corresponding sensitivity profiles (fold changes, FCs) induced by mutations are listed in Table 3. As shown, the sensitivity profiles of seven mutations reported in experimental studies[48,49] were successfully predicted by *in silico* site-directed mutagenesis analysis. Figure 3 illustrates that the values between FC_{calc} and FC_{exp} were in an excellent correlation (R^2 = 0.99). The excellent correlation was due to the high FC value of P655S mutation compared with the other mutations (Table 3), and

DOI: 10.1021/acschemneuro.8b00059
ACS Chem. Neurosci. 2018, 9, 1492−1502

Table 3. Comparison of Binding Free Energies Calculated by *in Silico* Mutagenesis Analysis (Contribution of Each Energy Term in eq 1 is Listed in SI, Table S2) of MPEP with Mutational Experiments (ΔG is in kcal/mol)

mutation site(s)	$\Delta\Delta G_{calc}$ [a]	ΔG_{mutant} [b]	FC_{calc} [c]	FC_{exp} [d]
P655S	2.35	−35.45	45.50	40.00
S658C	0.31	−37.49	1.65	0.90
P655S/S658C	1.56	−36.24	12.61	9.00
Y659F	−0.08	−37.88	0.88	0.80
L744V	0.96	−36.84	4.76	3.90
T781A	1.37	−36.43	9.26	4.60
Y792A	1.07	−36.73	5.69	4.90

[a] $\Delta\Delta G_{calc} = \Delta G_{mutant} - \Delta G_{wild\ type}$ ($\Delta G_{wild\ type}$ is the binding free energy of MPEP: −37.80 kcal/mol). [b] $\Delta G_{mutation}$ is the calculated binding free energies of mutation complexes. [c] Fold changes of potency measured by MD simulation (FC_{calc}) are derived from equation: $\Delta\Delta G_{calc} = RT\ln(FC_{calc})$. [d] $FC_{exp} = K_D(mutant)/K_D(wild\ type)$ reported from previous studies.[48]

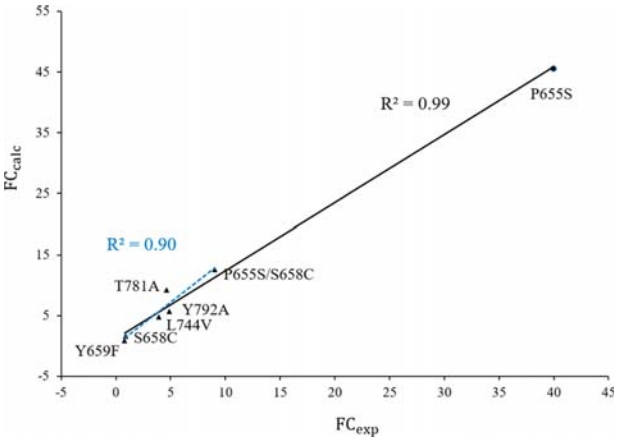

Figure 3. Graphical representation of correlation between the fold changes of simulation (FC_{calc}) and that of experiment (FC_{exp}) for mutant complexes. The correlation between FC_{calc} and FC_{exp} of seven mutations is indicated by the black solid line, and the correlation of six mutations (except for P655S mutation) is shown by the blue dashed line.

the values between FC_{calc} and FC_{exp} of the six mutations, except for P655S, still exhibited a good correlation (R^2 = 0.90). The high correlation between FC_{calc} and FC_{exp} as well as the distinct difference in FC values (ranging from 0.8 to 40) of sensitive mutations indicated that the constructed model was capable of distinguishing the sensitive mutations from the nonsensitive ones. Since all *in silico* site-directed mutagenesis was based on the wild type complexes, their ability to distinguish the sensitivity profiles of residues in $mGlu_5$ receptor could be used to test and validate the accuracy of our models constructed in this work. Furthermore, the conformational changes of $mGlu_5$ receptor binding site wherein MPEP located were also shown in SI, Figure S7.

Binding Mechanism of NAMs in the $mGlu_5$ Receptor. *Interactions Analysis between NAMs and the $mGlu_5$ Receptor.* The representative snapshots of five clinically important NAMs in $mGlu_5$ receptor with key interactions were presented in Figure 4. The allosteric binding site of $mGlu_5$ receptor was composed of three main regions including the lower chamber, the upper chamber, and a narrow channel between the two parts.[37] First, the aromatic rings (phenyl, pyridyl, and thiazole) of NAMs were surrounded by the lower chamber of binding site and mainly formed hydrophobic interactions with three residues ($I625^{2.46}$, $P655^{3.40}$, and $A810^{7.40}$) (Figure 4). For the basimglurant-$mGlu_5$ complex, the nitrogen of pyridyl also made a hydrogen bond interaction with $S658^{3.43}$ with a distance value of 2.4 Å. Second, the alkyne linkers and urea carbonyl of NAMs, crossing the narrow channel, mainly participated in interaction with $S809^{7.39}$. As shown, the hydroxyl oxygens of mavoglurant, the nitrogen in imidazole of basimglurant, and thiazole of STX107 also formed hydrogen bonds with the side chain of residue $S809^{7.39}$ in each complex (Figure 4A−D). Third, the bicyclic rings and imidazoline moiety of NAMs inserted into the upper chamber of the site defined primarily by nine residues ($I651^{3.36}$, $V740^{5.40}$, $L744^{5.44}$, $N747^{5.47}$, $W785^{6.50}$, $F788^{6.53}$, $M802^{7.32}$, $S805^{7.35}$, and $V806^{7.36}$). Except for the important hydrophobic interactions with nonpolar residues, $N747^{5.47}$ made a hydrogen bond contact with the carbamate tail of mavoglurant. Moreover, $N747^{5.47}$ and $I651^{3.36}$ also engaged in hydrogen bond with dipraglurant, STX107, and fenobam mediated by a water molecule (Figure 4B, D, and E). The water molecule from solvent flexibly shifted its position during MD simulation and mediated multiple hydrogen bonds between ligands and binding site in $mGlu_5$ receptor. This observed result was consistence with the study reported by Dalton et al.[50] that the water molecule also entered the allosteric site of $mGlu_5$ receptor from solvent. Water molecules from the solvent always impacted the ligand−receptor interactions according to the ligand property, and affected the flexibility of the protein.[51,52] In this study, the water molecule mediated the binding of NAMs to $mGlu_5$ receptor as well.

Per-Residue Energy Contribution Analysis of NAMs Binding to the $mGlu_5$ Receptor. To the best of our knowledge, Figure 5 provides a first panorama view that depicts the energy contributions of NAMs binding to $mGlu_5$ receptor at the per-residue basis (SI, Table S3 provides detailed information of per-residue energy contributions). As illustrated in Figure 5, 12, 14, 12, 13, and 12 residues were identified as high contribution ones (absolute energy contribution values ≥ 0.5 kcal/mol) for the binding of NAMs mavoglurant, dipraglurant, basimglurant, STX107, and fenobam to $mGlu_5$ receptor, respectively. Among them, there were three residues ($P655^{3.40}$, $L744^{5.44}$, and $V806^{7.36}$) whose energy contributions were significantly 24.91−33.56% among the whole complexes. Besides, the energy contributions of the same residue varied in different complexes and different residues' contribution in the same complexes were also inequable. For instance, the energy contribution of $N747^{5.47}$ to the binding of mavoglurant was −2.12 kcal/mol while basimglurant was only −0.10 kcal/mol. In mavoglurant-$mGlu_5$ complex, the energy contributions of residues in binding site ranged from −2.09 kcal/mol ($P655^{3.40}$) to −0.51 kcal/mol ($V740^{5.40}$). Overall, Figure 5 infers a certain level of similarity among the five clinical complexes, which inspired us to conduct a further characterization of the common features shared by NAMs-$mGlu_5$ recognition.

Common Features Shared by NAMs-$mGlu_5$ Recognition. The hierarchical clustering analysis of per-residue binding free energies was exploited to characterize the common features shared by clinically important NAMs in $mGlu_5$ receptor allosteric site. In SI, Figure S8, the distinct residues are clustered into five groups (A−E). As shown, the per-residue energy contributions of residues in group A were consistently higher than those of residues in groups B−E. It was estimated

DOI: 10.1021/acschemneuro.8b00059
ACS Chem. Neurosci. 2018, 9, 1492−1502

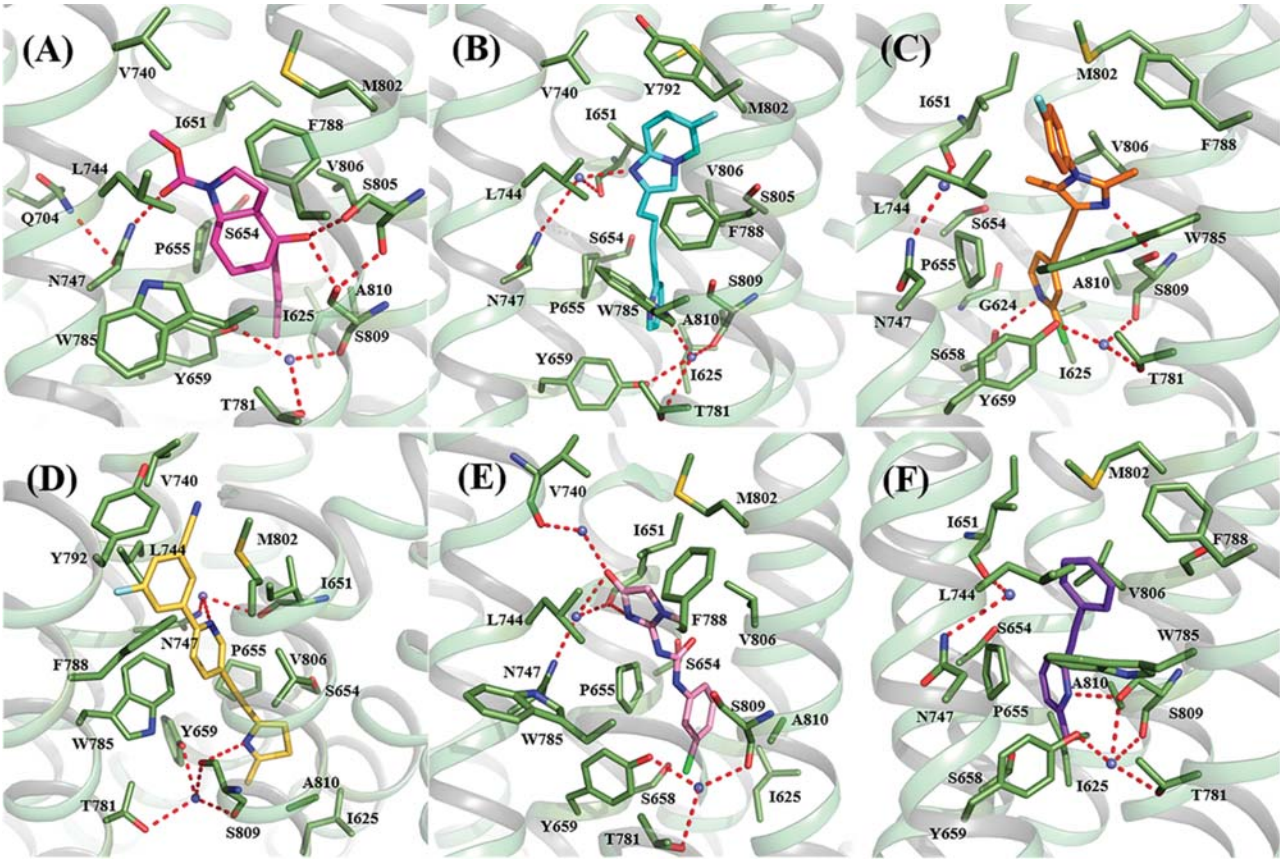

Figure 4. Representative structures of NAMs (A) mavoglurant, (B) dipraglurant, (C) basimglurant, (D) STX107, (E) fenobam, and (F) MPEP binding to allosteric site of the $mGlu_5$ receptor from equilibrated MD trajectories. The protein is shown in ribbon representation. The binding site residues and NAMs are shown as sticks. The hydrogen bond interactions are depicted as red dotted lines. The water molecules are displayed as purple balls.

that the residues in group A ($I625^{2.46}$, $I651^{3.36}$, $S654^{3.39}$, $P655^{3.40}$, $L744^{5.44}$, $W785^{6.50}$, $F788^{6.53}$, $M802^{7.32}$, $V806^{7.36}$, $S809^{7.39}$, and $A810^{7.40}$) assumed a large proportion in total contribution to five clinical NAMs binding with the percentages of 60.10−76.98%. In addition, some residues in group B ($G624^{2.45}$, $S658^{3.43}$, $Y659^{3.44}$, $V740^{5.40}$, $N747^{5.47}$, $Y792^{6.57}$, and $S805^{7.35}$) were also important contributors to the binding of NAMs. As a result, 11 residues ($I625^{2.46}$, $I651^{3.36}$, $S654^{3.39}$, $P655^{3.40}$, $L744^{5.44}$, $W785^{6.50}$, $F788^{6.53}$, $M802^{7.32}$, $V806^{7.36}$, $S809^{7.39}$, and $A810^{7.40}$) mainly located in TM2, TM3, TM5, TM6, and TM7 were characterized as the common features shared by NAMs-$mGlu_5$ recognition. Referring to the binding mode shown in Figure 4, the common features were further generalized and are schematically represented in SI, Figure S9. As shown, the chemical group R_1 of NAMs were surrounded by six residues ($I625^{2.46}$, $S654^{3.39}$, $P655^{3.40}$, $S658^{3.43}$, $Y659^{3.44}$, and $A810^{7.40}$). The linkers of NAMs crossed a narrow channel defined by four residues ($P655^{3.40}$, $Y659^{3.44}$, $V806^{7.36}$, and $S809^{7.39}$). The chemical groups R_2 of NAMs were mainly located in the site constituted by nine residues ($I651^{3.36}$, $V740^{5.40}$, $L744^{5.44}$, $N747^{5.47}$, $W785^{6.50}$, $F788^{6.53}$, $M802^{7.32}$, $S805^{7.35}$, and $V806^{7.36}$). Moreover, Figure 6 illustrates that the receptor-based pharmacophore models of the clinically important NAMs binding in $mGlu_5$ receptor. The pharmacophore of five clinical NAMs is shown in Figure 6A and B with the ligand−receptor interactions including hydrophobic interactions and hydrogen bonds. In Figure 6C, the interactions derived from the representative structures revealed that NAMs predominantly formed hydrophobic interactions with the binding site and made hydrogen bonds with four residues ($S658^{3.43}$, $N747^{5.47}$, $S805^{7.35}$, and $S809^{7.39}$). The pharmacophore models generated by superimposing the NAMs bound complexes were consistent with the identified common binding features in mGlu5 binding site for NAMs (SI, Figure S9).

Insights into Rational Drug Design. A major goal of the current work was to explore the binding mechanism of NAMs in $mGlu_5$ receptor and provided some useful information about the modification or the design of new potential NAMs. Our simulation results indicated that 11 residues located in TM2, TM3, TM5, TM6, and TM7 of $mGlu_5$ receptor were characterized as the common features shared by NAMs-$mGlu_5$ recognition. Among them, 82% of residues, belonging to nonpolar ones, suggested that the binding site was more beneficial to the binding of molecules with certain hydrophobic moieties. In addition, hydrogen bond interactions have been also discovered to be critical for enhancing binding affinities of NAMs. For instance, the five residues ($S658^{3.43}$, $Y659^{3.44}$, $N747^{5.47}$, $S805^{7.35}$, and $S809^{7.39}$) have often involved in hydrogen bond interactions with NAMs. Seeking to identify and optimize hydrogen bond interactions were also effective to provide structural stability for ligand−receptor complex.[53] Moreover, three residues with aromatic rings ($Y659^{3.44}$, $W785^{6.50}$, and $F788^{6.53}$) located in binding site were also involved in hydrophobic interactions. Since the $\pi-\pi$ stacking

DOI: 10.1021/acschemneuro.8b00059
ACS Chem. Neurosci. 2018, 9, 1492−1502

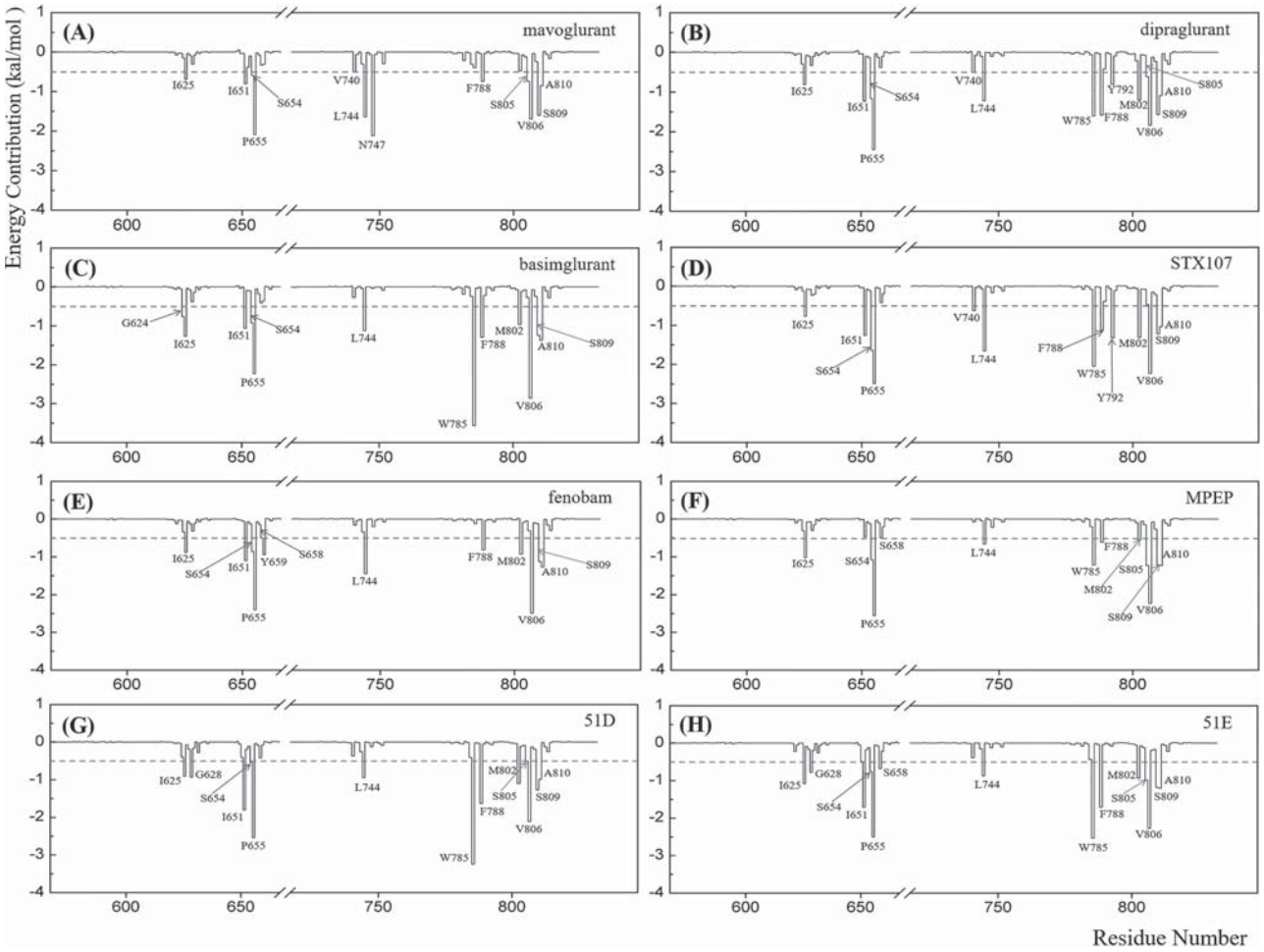

Figure 5. Per-residue binding free energy decomposition of eight NAMs (A) mavoglurant, (B) dipraglurant, (C) basimglurant, (D) STX107, (E) fenobam, (F) MPEP, (G) 51D, and (H) 51E binding to $mGlu_5$ receptor. Residues with high energy contribution (the absolute energy contribution values $\geq$ 0.5 kcal/mol) are labeled.

interaction was an attractive element to improve drug affinity and efficacy,[52] it was suggested that the rational drug design to introduce aromatic rings to NAMs within the appropriate distances and orientations and thus form $\pi-\pi$ stacking interaction with these residues (Y659$^{3.44}$, W785$^{6.50}$, and F788$^{6.53}$) may enhance the binding affinity of the designed or structurally modified NAMs.

CONCLUSION

In this work, the pharmacophores of NAMs participating in interactions within allosteric binding site of $mGlu_5$ receptor have been investigated by integrating multiple computational methods. The NAMs were docked into receptor using IFD approach and the obtained docking complexes were further assessed by MD simulations followed by binding free energy calculations. *In silico* site-directed mutagenesis analysis was performed to verify the simulation model. It was shown that the shared common features of the studied 5 clinically important NAMs (mavoglurant, dipraglurant, basimglurant, STX107, and fenobam) made contact with 11 residues located in allosteric site. The chemical group R_1 of NAMs were surrounded by six residues (I625$^{2.46}$, S654$^{3.39}$, P655$^{3.40}$, S658$^{3.43}$, Y659$^{3.44}$ and A810$^{7.40}$). The linker of NAMs crossed a narrow channel mainly defined by four residues (P655$^{3.40}$, Y659$^{3.44}$, V806$^{7.36}$, and S809$^{7.39}$). The chemical group R_2 of NAMs located in the site defined by nine residues (I651$^{3.36}$, V740$^{5.40}$, L744$^{5.44}$, N747$^{5.47}$, W785$^{6.50}$, F788$^{6.53}$, Met802$^{7.32}$, S805$^{7.35}$, and V806$^{7.36}$). The binding mechanism identified in this work would provide a basis for further development of novel NAMs targeting the $mGlu_5$ receptor.

METHODS

Prearation of Crystal Structures. Until now, only three crystal structures (PDB code 4OO9[1], 5CGC,[37] and 5CGD[37]) of the TM domain of $mGlu_5$ receptor are available in the PDB database. In this study, all three crystal structures were selected as the initial coordinates for the further MD simulations. The 4OO9 was released in 2014 at 2.6 Å resolution crystallized with mavoglurant.[1] The structure of mavoglurant is similar to that of the clinically important NAMs studied in this work (Figure 1). The 5CGC and 5CGD were determined in the presence of NAMs 51D (resolution: 3.1 Å) and 51E (resolution: 2.6 Å) by molecular replacement using the structure of 4OO9.[37] Except for TM domain residues (S568 to N832) of the receptor, ligands, and cocrystallized water molecules located in allosteric site, all other atoms in the three crystal structures were removed. The missing second intracellular (ICL2) and extracellular loops (ECL2) of three crystal structures were modeled and refined by using Prime.[54,55] Clustal was used to align sequences, and the

DOI: 10.1021/acschemneuro.8b00059
ACS Chem. Neurosci. 2018, 9, 1492−1502

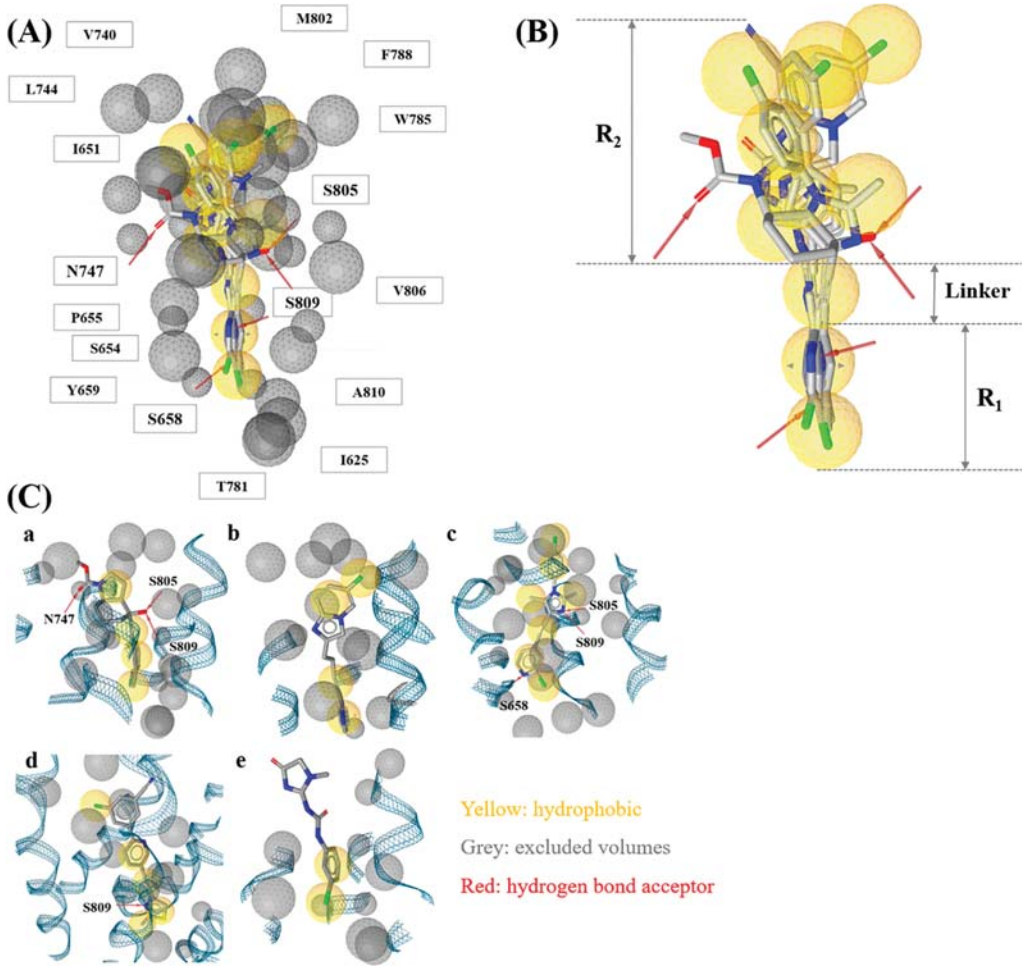

Figure 6. Pharmacophore based on the superimposition of the NAMs bound complexes. (A,B) Shared feature pharmacophores of NAMs in the receptor-binding and (C) pharmacophores of each NAM in the receptor-binding (a,b: mavoglurant, dipraglurant, basimglurant, STX107, and fenobam).

knowledge-based method was selected for building the missing structures.

Induced Fit Docking. As the structure of mavoglurant is similar to those of the clinically important NAMs studied in this work, the initial poses of the five NAMs (dipraglurant, basimglurant, fenobam, STX107, and MPEP) in receptors were obtained by the Induced Fit Docking (IFD) method[56] using the prepared mavoglurant-$mGlu_5$ complex as a template structure. The 3D structures of the five NAMs were achieved from the PubChem database,[57] and were prepared using LigPrep[58] with OPLS-2005 force field for energy minimization and with the ionized state assigned by Epik[59] at a pH value of 7.0 ± 2.0. Then, the Protein Preparation Wizard tool was applied to prepare the receptor structure. The size of the grid box was set by picking the original ligand mavoglurant in allosteric site of $mGlu_5$ receptor. In the IFD workflow, the Glide[60] standard precision (SP) docking was first applied, and then Prime[54] was used to refine the binding site residues within 5.0 Å of the ligand poses from the initial docking. Finally, 20 top-ranked poses of IFD docking conformation were predicted, and the poses with the most similar orientation of the original ligand mavoglurant were selected as their initial binding poses for further MD simulation.[42] Besides, mavoglurant was redocked into the allosteric binding site of $mGlu_5$ receptor using the same parameters and compared with the crystallized pose (PDB code 4OO9[1]) to validate the IFD protocol used in this work.[61]

Construction of Protein–Ligand and Membrane Complex. Eight complexes (three crystal structures and five IFD modeled structures) were first subjected to OPM[62] to calculate the spatial orientations respecting to the Membrane Normal defined by the *Z*-axis. Then, each of the complex was inserted into the explicit POPC lipid bilayer by using Membrane Builder in CHARMM-GUI.[63] Meanwhile, the complexes of protein, ligand, and lipids were immersed into TIP3P water[64] with 20.0 Å thickness.[65] Finally, according to the physiological ion concentration, the ionic concentrations of the systems were set to be 0.15 mol/L and neutralized by sodium and chloride ions.[66,67] As a result, each system contained ∼54 864 atoms per periodic cell with box size 95 Å × 86 Å × 113 Å.

MD Simulations. *Force Field Parameters of Protein, Lipids, and Ligand.* Before MD simulations, each of the systems was prepared by using LEaP.[68] AMBER ff14SB[69] and Lipid14[70] were used for protein and lipids to assign force field parameters. Disulfide bond between Cys644 and Cys733 of $mGlu_5$ receptor was also defined in each system. The force field parameters for ligands were generated using Antechamber program[71] with GAFF and RESP partial charges.[72,73] Geometric optimization and the electrostatic potential calculations of ligands were actualized at the HF/6-31G* level of the Gaussian09 suite.[74]

Energy Minimization, Equilibration, and Production Runs. All MD simulations were performed with GPU-accelerated NAMD (version 2.12).[75] To remove bad contacts between the solute and solvent water molecules, energy minimization and equilibration simulations were conducted before the production simulations. First, except for the lipid tail, all atoms were fixed to minimize 0.1 ns and

DOI: 10.1021/acschemneuro.8b00059
ACS Chem. Neurosci. 2018, 9, 1492−1502

equilibrate 0.5 ns. Second, each system with ligand heavy atoms, protein Cα atoms, and ions fixed was further minimized for 0.1 ns and equilibrated for 0.5 ns. Third, the entire system was all released to carry out 5 ns equilibrated MD simulation. Afterward, 100 ns production MD simulation for each system was conducted in NPT ensemble with a constant temperature of 310.0 K and a constant pressure of 1 bar. During simulations, periodic boundary conditions were employed and electrostatic calculations were based on the particle-mesh Ewald (PME)[76] method with a 10.0 Å nonbonded cutoff.[77] An integration step of 2 fs was used, and the coordinates of trajectory were saved every 5000 steps.

Analysis of the Simulation Trajectory. All of the MD trajectories analysis, such as the RMSD calculation and the extraction of representative snapshots, were performed by using CPPTRAJ.[78] The visualization of structures was performed with PyMOL.[79]

Binding Free Energy Analysis. Here, 500 snapshots taken from the last 50 ns equilibrium trajectory of each system were employed to calculate binding free energy (ΔG_{calc}) by the molecular mechanics/generalized Born surface area (MM/GBSA) method.[44] And the method has been successfully applied across a range of targets including GPCRs,[80,81] transporters,[82,83] enzymes,[84] and so on. For each snapshot, the binding free energy of ligand binding to $mGlu_5$ receptor was calculated by the following equation:

$$\Delta G_{calc(MM/GBSA)} = \Delta E_{vdW} + \Delta E_{ele} + \Delta G_{pol} + \Delta G_{nonpol} \quad (1)$$

The terms ΔE_{vdW} and ΔE_{ele} represented the van der Waals interaction and electrostatic contribution in the gas phase, respectively. Polar and nonpolar solvent interaction energies were expressed in ΔG_{pol} and ΔG_{nonpol}. ΔE_{vdW} and ΔE_{ele} were estimated using the force field ff14SB of AMBER,[69] and electrostatic free energy of solvation (ΔG_{pol}) was calculated by the modified GB model (igb = 2) developed by Onufriev et al.[85] The dielectric constants of solute and solvent were set to 1 and 80, respectively. $\Delta G_{nonpol} = 0.0072 \times \Delta SASA$ was used to calculated the ΔG_{nonpol}, and ΔSASA was estimated by linear combination of pairwise overlaps method (LCPO) with 1.4 Å probe radii.[86,87] To analyze the energy contribution of each residue, per-residue decomposed energy ($\Delta G_{calc}^{per-residue}$) was calculated according to the following equation:

$$\Delta G_{calc}^{per\text{-}residue} = \Delta E_{vdW}^{per\text{-}residue} + \Delta E_{ele}^{per\text{-}residue} + \Delta G_{pol}^{per\text{-}residue} + \Delta G_{nonpol}^{per\text{-}residue} \quad (2)$$

$\Delta E_{vdW}^{per\text{-}residue}$, $\Delta E_{ele}^{per\text{-}residue}$, and $\Delta G_{pol}^{per\text{-}residue}$ were the same terms as illustrated in eq 1. Moreover, the nonpolar solvation contribution in eq 2 was estimated according $\Delta G_{nonpol}^{per\text{-}residue} = 0.0072 \times \Delta SASA$, and the ΔSASA was obtained from the icosahedron (ICOSA) method.[88,89]

***In Silico* Site-Directed Mutagenesis Analysis.** *In silico* site-directed mutagenesis was carried out on the reported MPEP sensitive mutations to validate the accuracy of computational model in this study. Starting from the snapshots extracted from the equilibrated WT trajectory, a total of 7 mutant complexes (P655S, S658C, P655S–S658C, Y659F, L744V, T781A, Y792A) were generated by mutagenesis tool in PyMOL[79] and were processed by LEaP.[68] For each mutant system, short MD simulation (20 ns) and binding free energy calculation were implemented using the same procedures as depicted in "Energy Minimization, Equilibration, and Production Runs" and "Binding Free Energy Analysis" sections mentioned above.

Hierarchical Clustering Analysis of Per-residue Binding Free Energy. The hierarchical clustering tree of 132 residues with contributions to at least one clinical NAM binding to $mGlu_5$ receptor[47,90] was generated based on per-residue energy contribution vectors using *R* statistical analysis software[91] with the similarity levels among vectors measured by *Manhattan* distance:

$$\text{distance}(a, b) = \sum_i |a_i - b_i| \quad (3)$$

where *i* represents each dimension of per-residue energies *a* and *b*. The cluster algorithm applied here was based on the Ward's minimum variance method,[92,93] which was developed to minimize the total within-cluster variance. And the hierarchical tree graph was generated by the online tree generator iTOL.[94]

Pharmacophore Modeling. The 3D pharmacophore model of NAMs binding in $mGlu_5$ receptor was created with LigandScout 4.2 Advanced by automatically deriving key chemical features.[95] First, the representative structures of five clinically important NAMs were extracted from the MD trajectories. Then, the receptor-based pharmacophore of each NAM was automatically constructed with the hydrogen bonds, hydrophobic interactions, and excluded volumes. Finally, the pharmacophores were aligned to generate the shared feature pharmacophore of five clinically important NAMs binding in $mGlu_5$ receptor.

■ ASSOCIATED CONTENT

Supporting Information

The Supporting Information is available free of charge on the ACS Publications website at DOI: 10.1021/acschemneuro.8b00059.

(PDF)

■ AUTHOR INFORMATION

Corresponding Authors

*E-mail: xueww@cqu.edu.cn. Phone: +86-(0)23-65678468.
*E-mail: zhufeng.ns@gmail.com and zhufeng@zju.edu.cn. Phone: +86-(0)23-65678468.

ORCID

Yuzong Chen: 0000-0002-5473-8022
Xiaojun Yao: 0000-0002-8974-0173
Weiwei Xue: 0000-0002-3285-0574
Feng Zhu: 0000-0001-8069-0053

Author Contributions

W.X. and F.Z. designed the research. T.F., W.X., and F.Z. performed the research. T.F., G.Z., G.T., F.Y., W.X., X.Y., Y.C., and X.L. analyzed the data. T.F., W.X., and F.Z. wrote the manuscript. All authors reviewed the manuscript.

Funding

This work was funded by the National Natural Science Foundation of China (21505009); the Precision Medicine Project of the National Key Research and Development Plan of China (2016YFC0902200); Innovation Project on Industrial Generic Key Technologies of Chongqing (cstc2015zdcy-ztzx120003); and Fundamental Research Funds for Central Universities (10611CDJXZ238826, CDJZR14468801, CDJKXB14011).

Notes

The authors declare no competing financial interest.

■ ABBREVIATIONS

$mGlu_5$, metabotropic glutamate receptor 5; NAMs, negative allosteric modulators; PAMs, positive allosteric modulators; SAMs, silent allosteric modulators; CNS, central nervous system; MDD, major depressive disorder; FXS, fragile X syndrome; PD-LID, Parkinson's disease levodopa-induced dyskinesias; OCD, obsessive-compulsive disorder; MD, molecular dynamics; IFD, Induced Fit Docking; MM/GBSA, molecular mechanics/generalized Born surface area.

■ REFERENCES

(1) Dore, A. S., Okrasa, K., Patel, J. C., Serrano-Vega, M., Bennett, K., Cooke, R. M., Errey, J. C., Jazayeri, A., Khan, S., Tehan, B., Weir, M., Wiggin, G. R., and Marshall, F. H. (2014) Structure of class C GPCR

DOI: 10.1021/acschemneuro.8b00059
ACS Chem. Neurosci. 2018, 9, 1492−1502

metabotropic glutamate receptor 5 transmembrane domain. *Nature 511*, 557−562.
(2) Ribeiro, F. M., Vieira, L. B., Pires, R. G., Olmo, R. P., and Ferguson, S. S. (2017) Metabotropic glutamate receptors and neurodegenerative diseases. *Pharmacol. Res. 115*, 179−191.
(3) Niswender, C. M., and Conn, P. J. (2010) Metabotropic glutamate receptors: physiology, pharmacology, and disease. *Annu. Rev. Pharmacol. Toxicol. 50*, 295−322.
(4) Yang, H., Qin, C., Li, Y. H., Tao, L., Zhou, J., Yu, C. Y., Xu, F., Chen, Z., Zhu, F., and Chen, Y. Z. (2016) Therapeutic target database update 2016: enriched resource for bench to clinical drug target and targeted pathway information. *Nucleic Acids Res. 44*, D1069−D1074.
(5) Mukherjee, S., and Manahan-Vaughan, D. (2013) Role of metabotropic glutamate receptors in persistent forms of hippocampal plasticity and learning. *Neuropharmacology 66*, 65−81.
(6) Li, G., Jorgensen, M., Campbell, B. M., and Doller, D. (2016) Recent Developments in Group I Metabotropic Glutamate Receptor Allosteric Modulators for the Treatment of Psychiatric and Neurological Disorders (2014-May 2015). *Curr. Top. Med. Chem. 16*, 3470−3526.
(7) Niswender, C. M., Jones, C. K., and Conn, P. J. (2005) New therapeutic frontiers for metabotropic glutamate receptors. *Curr. Top. Med. Chem. 5*, 847−857.
(8) Li, Y. H., Yu, C. Y., Li, X. X., Zhang, P., Tang, J., Yang, Q., Fu, T., Zhang, X., Cui, X., Tu, G., Zhang, Y., Li, S., Yang, F., Sun, Q., Qin, C., Zeng, X., Chen, Z., Chen, Y. Z., and Zhu, F. (2018) Therapeutic target database update 2018: enriched resource for facilitating bench-to-clinic research of targeted therapeutics. *Nucleic Acids Res. 46*, D1121−D1127.
(9) Zhu, F., Li, X. X., Yang, S. Y., and Chen, Y. Z. (2018) Clinical Success of Drug Targets Prospectively Predicted by In Silico Study. *Trends Pharmacol. Sci. 39*, 229−231.
(10) Bailey, D. B., Jr., Berry-Kravis, E., Wheeler, A., Raspa, M., Merrien, F., Ricart, J., Koumaras, B., Rosenkranz, G., Tomlinson, M., von Raison, F., and Apostol, G. (2016) Mavoglurant in adolescents with fragile X syndrome: analysis of Clinical Global Impression-Improvement source data from a double-blind therapeutic study followed by an open-label, long-term extension study. *J. Neurodev. Disord. 8*, 1.
(11) Yan, Q. J., Rammal, M., Tranfaglia, M., and Bauchwitz, R. P. (2005) Suppression of two major Fragile X Syndrome mouse model phenotypes by the mGluR5 antagonist MPEP. *Neuropharmacology 49*, 1053−1066.
(12) Li, B., Tang, J., Yang, Q., Li, S., Cui, X., Li, Y., Chen, Y., Xue, W., Li, X., and Zhu, F. (2017) NOREVA: normalization and evaluation of MS-based metabolomics data. *Nucleic Acids Res. 45*, W162−W170.
(13) Rascol, O., Fox, S., Gasparini, F., Kenney, C., Di Paolo, T., and Gomez-Mancilla, B. (2014) Use of metabotropic glutamate 5-receptor antagonists for treatment of levodopa-induced dyskinesias. *Parkinsonism Relat Disord 20*, 947−956.
(14) Petrov, D., Pedros, I., de Lemos, M. L., Pallas, M., Canudas, A. M., Lazarowski, A., Beas-Zarate, C., Auladell, C., Folch, J., and Camins, A. (2014) Mavoglurant as a treatment for Parkinson's disease. *Expert Opin. Invest. Drugs 23*, 1165−1179.
(15) Rutrick, D., Stein, D. J., Subramanian, G., Smith, B., Fava, M., Hasler, G., Cha, J. H., Gasparini, F., Donchev, T., Ocwieja, M., Johns, D., and Gomez-Mancilla, B. (2017) Mavoglurant Augmentation in OCD Patients Resistant to Selective Serotonin Reuptake Inhibitors: A Proof-of-Concept, Randomized, Placebo-Controlled, Phase 2 Study,. *Adv. Ther. 34*, 524−541.
(16) Quiroz, J. A., Tamburri, P., Deptula, D., Banken, L., Beyer, U., Rabbia, M., Parkar, N., Fontoura, P., and Santarelli, L. (2016) Efficacy and Safety of Basimglurant as Adjunctive Therapy for Major Depression: A Randomized Clinical Trial,. *JAMA Psychiatry 73*, 675−684.
(17) Lindemann, L., Porter, R. H., Scharf, S. H., Kuennecke, B., Bruns, A., von Kienlin, M., Harrison, A. C., Paehler, A., Funk, C., Gloge, A., Schneider, M., Parrott, N. J., Polonchuk, L., Niederhauser, U., Morairty, S. R., Kilduff, T. S., Vieira, E., Kolczewski, S., Wichmann, J., Hartung, T., Honer, M., Borroni, E., Moreau, J. L., Prinssen, E., Spooren, W., Wettstein, J. G., and Jaeschke, G. (2015) Pharmacology of basimglurant (RO4917523, RG7090), a unique metabotropic glutamate receptor 5 negative allosteric modulator in clinical development for depression. *J. Pharmacol. Exp. Ther. 353*, 213−233.
(18) Leach, K., and Gregory, K. J. (2017) Molecular insights into allosteric modulation of Class C G protein-coupled receptors. *Pharmacol. Res. 116*, 105−118.
(19) Bennett, K. A., Dore, A. S., Christopher, J. A., Weiss, D. R., and Marshall, F. H. (2015) Structures of mGluRs shed light on the challenges of drug development of allosteric modulators. *Curr. Opin. Pharmacol. 20*, 1−7.
(20) Bian, Y., Feng, Z., Yang, P., and Xie, X. Q. (2017) Integrated In Silico Fragment-Based Drug Design: Case Study with Allosteric Modulators on Metabotropic Glutamate Receptor 5. *AAPS J. 19*, 1235−1248.
(21) Zhu, F., Zheng, C. J., Han, L. Y., Xie, B., Jia, J., Liu, X., Tammi, M. T., Yang, S. Y., Wei, Y. Q., and Chen, Y. Z. (2008) Trends in the exploration of anticancer targets and strategies in enhancing the efficacy of drug targeting. *Curr. Mol. Pharmacol 1*, 213−232.
(22) Zhu, F., Shi, Z., Qin, C., Tao, L., Liu, X., Xu, F., Zhang, L., Song, Y., Liu, X., Zhang, J., Han, B., Zhang, P., and Chen, Y. (2012) Therapeutic target database update 2012: a resource for facilitating target-oriented drug discovery. *Nucleic Acids Res. 40*, D1128−D1136.
(23) Lane, J. R., Abdul-Ridha, A., and Canals, M. (2013) Regulation of G protein-coupled receptors by allosteric ligands. *ACS Chem. Neurosci. 4*, 527−534.
(24) Wenthur, C. J., Gentry, P. R., Mathews, T. P., and Lindsley, C. W. (2014) Drugs for allosteric sites on receptors. *Annu. Rev. Pharmacol. Toxicol. 54*, 165−184.
(25) Lindsley, C. W. (2011) Special issue on the pharmacology and medicinal chemistry of allosteric modulators of metabotropic glutamate receptors (mGluRs). *ACS Chem. Neurosci. 2*, 379.
(26) Felts, A. S., Rodriguez, A. L., Blobaum, A. L., Morrison, R. D., Bates, B. S., Thompson Gray, A., Rook, J. M., Tantawy, M. N., Byers, F. W., Chang, S., Venable, D. F., Luscombe, V. B., Tamagnan, G. D., Niswender, C. M., Daniels, J. S., Jones, C. K., Conn, P. J., Lindsley, C. W., and Emmitte, K. A. (2017) Discovery of N-(5-Fluoropyridin-2-yl)-6-methyl-4-(pyrimidin-5-yloxy)picolinamide (VU0424238): A Novel Negative Allosteric Modulator of Metabotropic Glutamate Receptor Subtype 5 Selected for Clinical Evaluation,. *J. Med. Chem. 60*, 5072−5085.
(27) Emmitte, K. A. (2017) mGlu5 negative allosteric modulators: a patent review (2013−2016). *Expert Opin. Ther. Pat. 27*, 691−706.
(28) Gregory, K. J., Nguyen, E. D., Malosh, C., Mendenhall, J. L., Zic, J. Z., Bates, B. S., Noetzel, M. J., Squire, E. F., Turner, E. M., Rook, J. M., Emmitte, K. A., Stauffer, S. R., Lindsley, C. W., Meiler, J., and Conn, P. J. (2014) Identification of specific ligand-receptor interactions that govern binding and cooperativity of diverse modulators to a common metabotropic glutamate receptor 5 allosteric site. *ACS Chem. Neurosci. 5*, 282−295.
(29) Jaeschke, G., Kolczewski, S., Spooren, W., Vieira, E., Bitter-Stoll, N., Boissin, P., Borroni, E., Buttelmann, B., Ceccarelli, S., Clemann, N., David, B., Funk, C., Guba, W., Harrison, A., Hartung, T., Honer, M., Huwyler, J., Kuratli, M., Niederhauser, U., Pahler, A., Peters, J. U., Petersen, A., Prinssen, E., Ricci, A., Rueher, D., Rueher, M., Schneider, M., Spurr, P., Stoll, T., Tannler, D., Wichmann, J., Porter, R. H., Wettstein, J. G., and Lindemann, L. (2015) Metabotropic glutamate receptor 5 negative allosteric modulators: discovery of 2-chloro-4-[1-(4-fluorophenyl)-2,5-dimethyl-1H-imidazol-4-ylethynyl]pyridine (basimglurant, RO4917523), a promising novel medicine for psychiatric diseases. *J. Med. Chem. 58*, 1358−1371.
(30) Urwyler, S. (2011) Allosteric modulation of family C G-protein-coupled receptors: from molecular insights to therapeutic perspectives. *Pharmacol Rev. 63*, 59−126.
(31) Galambos, J., Wagner, G., Nogradi, K., Bielik, A., Molnar, L., Bobok, A., Horvath, A., Kiss, B., Kolok, S., Nagy, J., Kurko, D., Bakk, M. L., Vastag, M., Saghy, K., Gyertyan, I., Gal, K., Greiner, I., Szombathelyi, Z., Keseru, G. M., and Domany, G. (2010)

DOI: 10.1021/acschemneuro.8b00059
ACS Chem. Neurosci. 2018, 9, 1492−1502

Carbamoyloximes as novel non-competitive mGlu5 receptor antagonists. *Bioorg. Med. Chem. Lett. 20*, 4371−4375.
(32) Felts, A. S., Rodriguez, A. L., Morrison, R. D., Bollinger, K. A., Venable, D. F., Blobaum, A. L., Byers, F. W., Thompson Gray, A., Daniels, J. S., Niswender, C. M., Jones, C. K., Conn, P. J., Lindsley, C. W., and Emmitte, K. A. (2017) Discovery of imidazo[1,2-a]-, [1,2,4]triazolo[4,3-a]-, and [1,2,4]triazolo[1,5-a]pyridine-8-carboxamide negative allosteric modulators of metabotropic glutamate receptor subtype 5. *Bioorg. Med. Chem. Lett. 27*, 4858−4866.
(33) Conn, P. J., Lindsley, C. W., Meiler, J., and Niswender, C. M. (2014) Opportunities and challenges in the discovery of allosteric modulators of GPCRs for treating CNS disorders. *Nat. Rev. Drug Discovery 13*, 692−708.
(34) Melancon, B. J., Hopkins, C. R., Wood, M. R., Emmitte, K. A., Niswender, C. M., Christopoulos, A., Conn, P. J., and Lindsley, C. W. (2012) Allosteric modulation of seven transmembrane spanning receptors: theory, practice, and opportunities for central nervous system drug discovery. *J. Med. Chem. 55*, 1445−1464.
(35) Jia, J., Zhu, F., Ma, X., Cao, Z., Li, Y., and Chen, Y. (2009) Mechanisms of drug combinations: interaction and network perspectives. *Nat. Rev. Drug Discovery 8*, 111−128.
(36) Galambos, J., Bielik, A., Wagner, G., Domany, G., Koti, J., Beni, Z., Szigetvari, A., Santa, Z., Orgovan, Z., Bobok, A., Kiss, B., Miko-Bakk, M. L., Vastag, M., Saghy, K., Krasavin, M., Gal, K., Greiner, I., Szombathelyi, Z., and Keseru, G. M. (2017) Discovery of 4-amino-3-arylsulfoquinolines, a novel non-acetylenic chemotype of metabotropic glutamate 5 (mGlu5) receptor negative allosteric modulators. *Eur. J. Med. Chem. 133*, 240−254.
(37) Christopher, J. A., Aves, S. J., Bennett, K. A., Dore, A. S., Errey, J. C., Jazayeri, A., Marshall, F. H., Okrasa, K., Serrano-Vega, M. J., Tehan, B. G., Wiggin, G. R., and Congreve, M. (2015) Fragment and Structure-Based Drug Discovery for a Class C GPCR: Discovery of the mGlu5 Negative Allosteric Modulator HTL14242 (3-Chloro-5-[6-(5-fluoropyridin-2-yl)pyrimidin-4-yl]benzonitrile). *J. Med. Chem. 58*, 6653−6664.
(38) Yu, C. Y., Li, X. X., Yang, H., Li, Y. H., Xue, W. W., Chen, Y. Z., Tao, L., and Zhu, F. (2018) Assessing the Performances of Protein Function Prediction Algorithms from the Perspectives of Identification Accuracy and False Discovery Rate. *Int. J. Mol. Sci. 19*, 183.
(39) Li, Y. H., Wang, P. P., Li, X. X., Yu, C. Y., Yang, H., Zhou, J., Xue, W. W., Tan, J., and Zhu, F. (2016) The Human Kinome Targeted by FDA Approved Multi-Target Drugs and Combination Products: A Comparative Study from the Drug-Target Interaction Network Perspective. *PLoS One 11*, e0165737.
(40) Dalton, J. A., Gomez-Santacana, X., Llebaria, A., and Giraldo, J. (2014) Computational analysis of negative and positive allosteric modulator binding and function in metabotropic glutamate receptor 5 (in)activation. *J. Chem. Inf. Model. 54*, 1476−1487.
(41) Anighoro, A., Graziani, D., Bettinelli, I., Cilia, A., De Toma, C., Longhi, M., Mangiarotti, F., Menegon, S., Pirona, L., Poggesi, E., Riva, C., and Rastelli, G. (2015) Insights into the interaction of negative allosteric modulators with the metabotropic glutamate receptor 5: discovery and computational modeling of a new series of ligands with nanomolar affinity. *Bioorg. Med. Chem. 23*, 3040−3058.
(42) Wang, P., Yang, F., Yang, H., Xu, X., Liu, D., Xue, W., and Zhu, F. (2015) Identification of dual active agents targeting 5-HT1A and SERT by combinatorial virtual screening methods. *Bio-Med. Mater. Eng. 26*, S2233−2239.
(43) Xu, J., Wang, P., Yang, H., Zhou, J., Li, Y., Li, X., Xue, W., Yu, C., Tian, Y., and Zhu, F. (2016) Comparison of FDA Approved Kinase Targets to Clinical Trial Ones: Insights from Their System Profiles and Drug-Target Interaction Networks. *BioMed Res. Int. 2016*, 2509385.
(44) Chen, F., Liu, H., Sun, H., Pan, P., Li, Y., Li, D., and Hou, T. (2016) Assessing the performance of the MM/PBSA and MM/GBSA methods. 6. Capability to predict protein-protein binding free energies and re-rank binding poses generated by protein-protein docking. *Phys. Chem. Chem. Phys. 18*, 22129−22139.
(45) Yang, F. Y., Fu, T. T., Zhang, X. Y., Hu, J., Xue, W. W., Zheng, G. X., Li, B., Li, Y. H., Yao, X. J., and Zhu, F. (2017) Comparison of computational model and X-ray crystal structure of human serotonin transporter: potential application for the pharmacology of human monoamine transporters. *Mol. Simul. 43*, 1089−1098.
(46) Li, B., Tang, J., Yang, Q. X., Cui, X. J., Li, S., Chen, S. J., Cao, Q. X., Xue, W. W., Chen, N., and Zhu, F. (2016) Performance evaluation and online realization of data-driven normalization methods used in LC/MS based untargeted metabolomics analysis. *Sci. Rep. 6*, 38881.
(47) Xue, W., Yang, F., Wang, P., Zheng, G., Chen, Y., Yao, X., and Zhu, F. (2018) What Contributes to Serotonin-Norepinephrine Reuptake Inhibitors' Dual-Targeting Mechanism? The Key Role of Transmembrane Domain 6 in Human Serotonin and Norepinephrine Transporters Revealed by Molecular Dynamics Simulation. *ACS Chem. Neurosci.*, DOI: 10.1021/acschemneuro.7b00490.
(48) Malherbe, P., Kratochwil, N., Zenner, M. T., Piussi, J., Diener, C., Kratzeisen, C., Fischer, C., and Porter, R. H. (2003) Mutational analysis and molecular modeling of the binding pocket of the metabotropic glutamate 5 receptor negative modulator 2-methyl-6-(phenylethynyl)-pyridine. *Mol. Pharmacol. 64*, 823−832.
(49) Malherbe, P., Kratochwil, N., Muhlemann, A., Zenner, M. T., Fischer, C., Stahl, M., Gerber, P. R., Jaeschke, G., and Porter, R. H. (2006) Comparison of the binding pockets of two chemically unrelated allosteric antagonists of the mGlu5 receptor and identification of crucial residues involved in the inverse agonism of MPEP. *J. Neurochem. 98*, 601−615.
(50) Dalton, J. A., Lans, I., Rovira, X., Malhaire, F., Gomez-Santacana, X., Pittolo, S., Gorostiza, P., Llebaria, A., Goudet, C., Pin, J. P., and Giraldo, J. (2016) Shining Light on an mGlu5 Photoswitchable NAM: A Theoretical Perspective. *Curr. Neuropharmacol. 14*, 441−454.
(51) Bortolato, A., Tehan, B. G., Bodnarchuk, M. S., Essex, J. W., and Mason, J. S. (2013) Water network perturbation in ligand binding: adenosine A(2A) antagonists as a case study. *J. Chem. Inf. Model. 53*, 1700−1713.
(52) Bissantz, C., Kuhn, B., and Stahl, M. (2010) A medicinal chemist's guide to molecular interactions,. *J. Med. Chem. 53*, 5061−5084.
(53) Ruiz-Carmona, S., Schmidtke, P., Luque, F. J., Baker, L., Matassova, N., Davis, B., Roughley, S., Murray, J., Hubbard, R., and Barril, X. (2017) Dynamic undocking and the quasi-bound state as tools for drug discovery. *Nat. Chem. 9*, 201−206.
(54) *Prime v. 2.0*, Schrödinger, LLC, New York, 2009.
(55) Li, Y. H., Xu, J. Y., Tao, L., Li, X. F., Li, S., Zeng, X., Chen, S. Y., Zhang, P., Qin, C., Zhang, C., Chen, Z., Zhu, F., and Chen, Y. Z. (2016) A Web-Server for Machine Learning Prediction of Protein Functional Families from Sequence Irrespective of Similarity. *PLoS One 11*, e0155290.
(56) *Induced Fit Docking protocol*, Schrödinger Suite, 2009.
(57) Kim, S., Thiessen, P. A., Bolton, E. E., Chen, J., Fu, G., Gindulyte, A., Han, L., He, J., He, S., Shoemaker, B. A., Wang, J., Yu, B., Zhang, J., and Bryant, S. H. (2016) PubChem Substance and Compound databases. *Nucleic Acids Res. 44*, D1202−D1213.
(58) *LigPrep v. 2.3*, Schrödinger, LLC, New York, 2009.
(59) *Epik v. 2.0*, Schrödinger, LLC, New York, 2009.
(60) *Glide v. 5.5*, Schrödinger, LLC, New York, 2009.
(61) Ikemori-Kawada, M., Inoue, A., Goto, M., Wang, Y. J., and Kawakami, Y. (2012) Docking simulation study and kinase selectivity of f152A1 and its analogs. *J. Chem. Inf. Model. 52*, 2059−2068.
(62) Lomize, M. A., Pogozheva, I. D., Joo, H., Mosberg, H. I., and Lomize, A. L. (2012) OPM database and PPM web server: resources for positioning of proteins in membranes. *Nucleic Acids Res. 40*, D370−D376.
(63) Wu, E. L., Cheng, X., Jo, S., Rui, H., Song, K. C., Davila-Contreras, E. M., Qi, Y., Lee, J., Monje-Galvan, V., Venable, R. M., Klauda, J. B., and Im, W. (2014) CHARMM-GUI Membrane Builder toward realistic biological membrane simulations. *J. Comput. Chem. 35*, 1997−2004.

DOI: 10.1021/acschemneuro.8b00059
ACS Chem. Neurosci. 2018, 9, 1492−1502

(64) Jorgensen, W. L., Chandrasekhar, J., Madura, J. D., Impey, R. W., and Klein, M. L. (1983) Comparison of simple potential functions for simulating liquid water. *J. Chem. Phys. 79*, 926−935.
(65) Zheng, G., Xue, W., Yang, F., Zhang, Y., Chen, Y., Yao, X., and Zhu, F. (2017) Revealing vilazodone's binding mechanism underlying its partial agonism to the 5-HT1A receptor in the treatment of major depressive disorder. *Phys. Chem. Chem. Phys. 19*, 28885−28896.
(66) Bai, Q., and Yao, X. (2016) Investigation of allosteric modulation mechanism of metabotropic glutamate receptor 1 by molecular dynamics simulations, free energy and weak interaction analysis. *Sci. Rep. 6*, 21763.
(67) Rao, H. B., Zhu, F., Yang, G. B., Li, Z. R., and Chen, Y. Z. (2011) Update of PROFEAT: a web server for computing structural and physicochemical features of proteins and peptides from amino acid sequence. *Nucleic Acids Res. 39*, W385−W390.
(68) Yang, L., Skjevik, A. A., Han Du, W. G., Noodleman, L., Walker, R. C., and Gotz, A. W. (2016) Data for molecular dynamics simulations of B-type cytochrome c oxidase with the Amber force field. *Data Brief 8*, 1209−1214.
(69) Maier, J. A., Martinez, C., Kasavajhala, K., Wickstrom, L., Hauser, K. E., and Simmerling, C. (2015) ff14SB: Improving the Accuracy of Protein Side Chain and Backbone Parameters from ff99SB. *J. Chem. Theory Comput. 11*, 3696−3713.
(70) Dickson, C. J., Madej, B. D., Skjevik, A. A., Betz, R. M., Teigen, K., Gould, I. R., and Walker, R. C. (2014) Lipid14: The Amber Lipid Force Field,. *J. Chem. Theory Comput. 10*, 865−879.
(71) Wang, J., Wang, W., Kollman, P. A., and Case, D. A. (2006) Automatic atom type and bond type perception in molecular mechanical calculations. *J. Mol. Graphics Modell. 25*, 247−260.
(72) Wang, J., Wolf, R. M., Caldwell, J. W., Kollman, P. A., and Case, D. A. (2004) Development and testing of a general amber force field. *J. Comput. Chem. 25*, 1157−1174.
(73) Bayly, C. I., Cieplak, P., Cornell, W., and Kollman, P. A. (1993) A well-behaved electrostatic potential based method using charge restraints for deriving atomic charges: the RESP model,. *J. Phys. Chem. 97*, 10269−10280.
(74) *Gaussian 09 v. D.01*; Gaussian, Inc., Wallingford, CT, 2009.
(75) Phillips, J. C., Braun, R., Wang, W., Gumbart, J., Tajkhorshid, E., Villa, E., Chipot, C., Skeel, R. D., Kale, L., and Schulten, K. (2005) Scalable molecular dynamics with NAMD. *J. Comput. Chem. 26*, 1781−1802.
(76) Darden, T., York, D., and Pedersen, L. (1993) Particle mesh Ewald: An N·log(N) method for Ewald sums in large systems. *J. Chem. Phys. 98*, 10089−10092.
(77) Xue, W., Wang, P., Tu, G., Yang, F., Zheng, G., Li, X., Li, X., Chen, Y., Yao, X., and Zhu, F. (2018) Computational identification of the binding mechanism of a triple reuptake inhibitor amitifadine for the treatment of major depressive disorder. *Phys. Chem. Chem. Phys. 20*, 6606−6616.
(78) Roe, D. R., and Cheatham, T. E., 3rd (2013) PTRAJ and CPPTRAJ: Software for Processing and Analysis of Molecular Dynamics Trajectory Data. *J. Chem. Theory Comput. 9*, 3084−3095.
(79) *PyMOL Molecular Graphics System v. 1.3*, Schrödinger, LLC.
(80) McRobb, F. M., Negri, A., Beuming, T., and Sherman, W. (2016) Molecular dynamics techniques for modeling G protein-coupled receptors. *Curr. Opin. Pharmacol. 30*, 69−75.
(81) Mendez-Luna, D., Bello, M., and Correa-Basurto, J. (2016) Understanding the molecular basis of agonist/antagonist mechanism of GPER1/GPR30 through structural and energetic analyses. *J. Steroid Biochem. Mol. Biol. 158*, 104−116.
(82) Xue, W., Wang, P., Li, B., Li, Y., Xu, X., Yang, F., Yao, X., Chen, Y. Z., Xu, F., and Zhu, F. (2016) Identification of the inhibitory mechanism of FDA approved selective serotonin reuptake inhibitors: an insight from molecular dynamics simulation study. *Phys. Chem. Chem. Phys. 18*, 3260−3271.
(83) Wang, P., Fu, T., Zhang, X., Yang, F., Zheng, G., Xue, W., Chen, Y., Yao, X., and Zhu, F. (2017) Differentiating physicochemical properties between NDRIs and sNRIs clinically important for the treatment of ADHD. *Biochim. Biophys. Acta, Gen. Subj. 1861*, 2766−2777.
(84) Zhu, F., Han, L. Y., Zheng, C. J., Xie, B., Tammi, M. T., Yang, S. Y., Wei, Y. Q., and Chen, Y. Z. (2009) What are next generation innovative therapeutic targets? Clues from genetic, structural, physicochemical and system profile of successful targets. *J. Pharmacol. Exp. Ther. 330*, 304−315.
(85) Onufriev, A., Bashford, D., and Case, D. A. (2004) Exploring protein native states and large-scale conformational changes with a modified generalized born model. *Proteins: Struct., Funct., Genet. 55*, 383−394.
(86) Weiser, J., Shenkin, P. S., and Still, W. C. (1999) Approximate atomic surfaces from linear combinations of pairwise overlaps (LCPO). *J. Comput. Chem. 20*, 217−230.
(87) Wang, P., Zhang, X., Fu, T., Li, S., Li, B., Xue, W., Yao, X., Chen, Y., and Zhu, F. (2017) Differentiating Physicochemical Properties between Addictive and Nonaddictive ADHD Drugs Revealed by Molecular Dynamics Simulation Studies. *ACS Chem. Neurosci. 8*, 1416−1428.
(88) *AMBER v. 14*, University of California, San Francisco, 2014.
(89) Zheng, G., Xue, W., Wang, P., Yang, F., Li, B., Li, X., Li, Y., Yao, X., and Zhu, F. (2016) Exploring the Inhibitory Mechanism of Approved Selective Norepinephrine Reuptake Inhibitors and Reboxetine Enantiomers by Molecular Dynamics Study. *Sci. Rep. 6*, 26883.
(90) Zhu, F., Qin, C., Tao, L., Liu, X., Shi, Z., Ma, X., Jia, J., Tan, Y., Cui, C., Lin, J., Tan, C., Jiang, Y., and Chen, Y. (2011) Clustered patterns of species origins of nature-derived drugs and clues for future bioprospecting. *Proc. Natl. Acad. Sci. U. S. A. 108*, 12943−12948.
(91) Tippmann, S. (2014) Programming tools: Adventures with R. *Nature 517*, 109−110.
(92) Szekely, G. J., and Rizzo, M. L. (2005) Hierarchical Clustering via Joint Between-Within Distances: Extending Ward's Minimum Variance Method. *Journal of Classification 22*, 151−183.
(93) Barer, M. R., and Harwood, C. R. (1999) Bacterial viability and culturability. *Adv. Microb. Physiol. 41*, 93−137.
(94) Letunic, I., and Bork, P. (2016) Interactive tree of life (iTOL) v3: an online tool for the display and annotation of phylogenetic and other trees. *Nucleic Acids Res. 44*, W242−W245.
(95) Wolber, G., and Langer, T. (2005) LigandScout: 3-D pharmacophores derived from protein-bound ligands and their use as virtual screening filters. *J. Chem. Inf. Model. 45*, 160−169.
(96) Emmitte, K. A. (2013) mGlu5 negative allosteric modulators: a patent review (2010−2012). *Expert Opin. Ther. Pat. 23*, 393−408.

DOI: 10.1021/acschemneuro.8b00059
ACS Chem. Neurosci. 2018, 9, 1492−1502